Direct Observations of the Evolution of Polar Cap Ionization Patches

Qing-He Zhang *et al.*

Science **339**, 1597 (2013);
DOI: 10.1126/science.1231487

Science (print ISSN 0036-8075; online ISSN 1095-9203) is published weekly, except the last week in December, by the American Association for the Advancement of Science, 1200 New York Avenue NW, Washington, DC 20005.

Direct Observations of the Evolution of Polar Cap Ionization Patches

Qing-He Zhang,[1]* Bei-Chen Zhang,[1] Michael Lockwood,[2] Hong-Qiao Hu,[1] Jøran Moen,[3] J. Michael Ruohoniemi,[4] Evan G. Thomas,[4] Shun-Rong Zhang,[5] Hui-Gen Yang,[1] Rui-Yuan Liu,[1] Kathryn A. McWilliams,[6,2] Joseph B. H. Baker[4]

Patches of ionization are common in the polar ionosphere, where their motion and associated density gradients give variable disturbances to high-frequency (HF) radio communications, over-the-horizon radar location errors, and disruption and errors to satellite navigation and communication. Their formation and evolution are poorly understood, particularly under disturbed space weather conditions. We report direct observations of the full evolution of patches during a geomagnetic storm, including formation, polar cap entry, transpolar evolution, polar cap exit, and sunward return flow. Our observations show that modulation of nightside reconnection in the substorm cycle of the magnetosphere helps form the gaps between patches where steady convection would give a "tongue" of ionization (TOI).

Polar cap patches are islands of high number-density F region ionospheric plasma, poleward of the auroral oval, surrounded by plasma of half the density or less (*1*, *2*). Previous theories and observations indicated that patches are formed by ionospheric dynamics in the "cusp region" (*3*–*8*), in which one mechanism considered to be dominant, at least in the European sector (*2*), is associated with magnetic reconnection between a (draped) southward interplanetary magnetic field (IMF) and the geomagnetic field at the dayside magnetopause. Patches follow the flow streamlines of the Dungey convection cycle (*9*), moving across the pole from the dayside to the nightside (*10*, *11*), and have been seen exiting the polar cap and entering the nightside auroral oval (*5*, *12*). It has long been recognized that mid-latitude ionospheric plasma, produced by solar extreme ultraviolet (EUV) radiation, provides a viable reservoir of source plasma, although in some cases densities may be further enhanced by precipitation of solar wind particles precipitating into the cusp ionosphere (*8*, *10*, *13*, *14*). Flow into the polar cap is restricted to a convection "throat" that, like the cusp precipitation, extends along the line in the ionosphere that is the magnetic footprint of the magnetopause reconnection (*14*).

Sometimes the enhanced ionization entering the polar cap takes the form of a continuous "tongue" of ionization (TOI) (*15*), rather than discrete patches, and numerical simulations readily reproduce a TOI by convecting solar-EUV–enhanced plasma antisunward through the throat (*16*). There has been considerable debate about why a TOI is not the usual occurrence, and a number of mechanisms that divide it up into patches have been proposed (*4*–*6*), with implications for a variety of operational systems (*2*, *17*). In addition, the convection that causes the motion of patches is not usually steady; rather, it varies with the substorm cycle (*9*) as the magnetic field accumulates and is then released in the tail of the magnetosphere (*18*), but the effect on patch evolution has not been observed. It has been particularly difficult to study the detailed motion and evolution of patches because of poor data coverage. Although there are two-dimensional (2D) trajectory analysis codes and 3D ionospheric assimilation techniques (*17*, *19*), neither has provided complete information. Here, we present continuous monitoring of both the plasma density and flow in a large fraction of the Northern Hemisphere convection zone over a full convection cycle (4 hours, with time resolution of 5 min) by combining the observations of the total electron content (TEC) (*20*) from the large and dense array of Global Positioning System (GPS) receivers (*21*, *22*) with the large-scale coverage of the flows provided by the Super Dual Auroral Radar Network (SuperDARN) radars using the Map Potential technique (*23*, *24*).

On 24 September 2011, a coronal mass ejection (CME) emerged from an active region on the Sun. This reached Earth's magnetopause 2 days later at 12:37 UT, giving an enhancement of solar wind dynamic pressure, P_{Dyn}. Geomagnetic indices reveal that this produced a major disturbance (a magnetic storm), the ap planetary geomagnetic

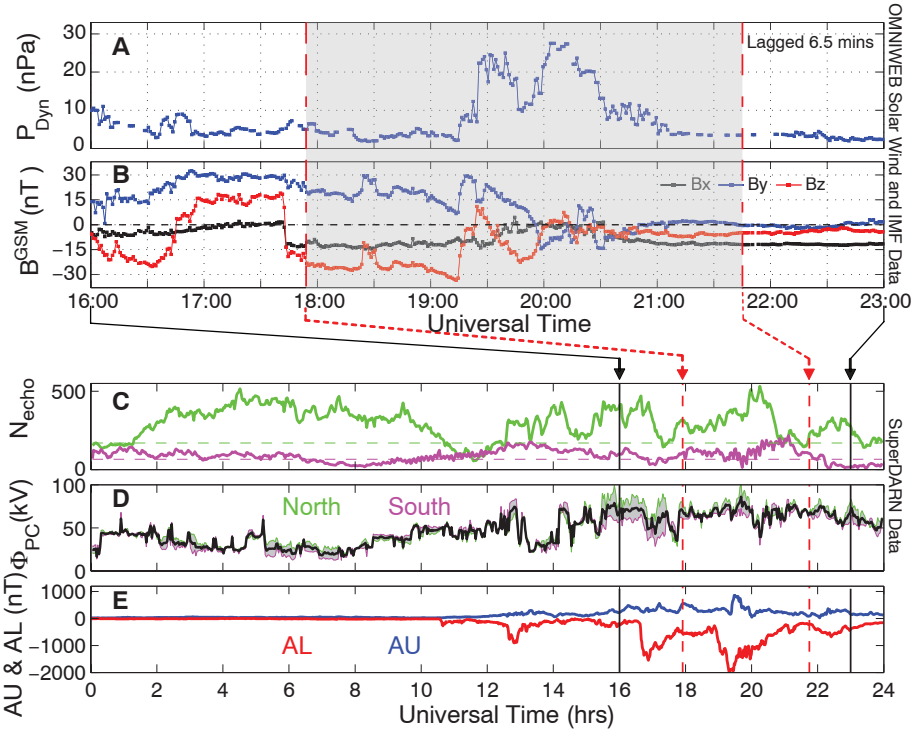

Fig. 1. An overview of the interplanetary conditions, the SuperDARN radar data, and the auroral electrojet (AE) indices on 26 September 2011. Parameters shown are (**A**) the solar wind dynamic pressure, P_{Dyn}; (**B**) the IMF components in GSM coordinates; (**C**) the number of valid Doppler shift values N_{echo} in each 2-min convection pattern from the SuperDARN radar networks (green/mauve lines are for the Northern/Southern Hemispheres, and horizontal dashed lines are the averages for 1998 to 2012: For much of the period of interest, the SuperDARN data are in the top 20% in terms of quality indicated by N_{echo}); (**D**) the transpolar voltage Φ_{PC} from the SuperDARN radars (the black line is the average for the Northern and Southern Hemispheres, and the gray area gives the difference between the hemispheric values); (**E**) the provisional AE auroral electrojet indices from 11 stations: The blue line is AU (auroral upper) and the red line is AL (auroral lower). Interplanetary data have been lagged to the nose of the magnetosphere using THEMIS-A (Time History of Events and Macroscale Interactions during Substorms–A) observations (fig. S1).

[1]State Oceanic Administration People's Republic of China Key Laboratory for Polar Science, Polar Research Institute of China, Shanghai, China. [2]Department of Meteorology, University of Reading, Earley Gate, Post Office Box 243, RG6 6BB, UK. [3]Department of Physics, University of Oslo, Blindern, Oslo, Norway. [4]Bradley Department of Electrical and Computer Engineering, Virginia Tech, Blacksburg, VA, USA. [5]Massachusetts Institute of Technology (MIT), Haystack Observatory, Westford, MA 01886, USA. [6]Institute of Space and Atmospheric Studies, University of Saskatchewan, Saskatoon, Saskatchewan, Canada.

*Corresponding author. E-mail: zhangqinghe@pric.gov.cn

index (see supplementary materials) reaching 94 at 15 to 21 UT (a level exceeded less than 0.5% of the time). A second enhancement in P_{Dyn} impacted the magnetosphere at about 19:15 UT (Fig. 1A). There was a large and variable IMF at Earth, with two intervals of an exceptionally strong southward field (B_Z, in red in Fig. 1B) ahead of this second P_{Dyn} pulse. This IMF orientation favors rapid reconnection at the dayside magnetopause and gave the growth phases of two substorms that ended with the onset of their expansion phases at 16:35 and 18:54 UT [AL (auroral lower) subsequently falling to –1500 nT and –2000 nT, respectively (Fig. 1D)]. The presence of substorms reveals intervals of dominant magnetopause reconnection followed by dominant magnetotail reconnection, and polar ionospheric convection is then predicted by the expanding-contracting polar cap (ECPC) model (*18*). Numerical modeling of the response to an isolated pulse of southward IMF using ECPC has shown that an initially localized convection enhancement on the dayside expands antisunward (*14*). However if, as in this case, a southward turning follows a previous one, a somewhat more global response of the convection pattern is expected (*25*) and, consistent with this modeling, the second southward turning of the IMF yielded an almost immediate rise in the transpolar voltage at 17:55 UT (Fig. 1D).

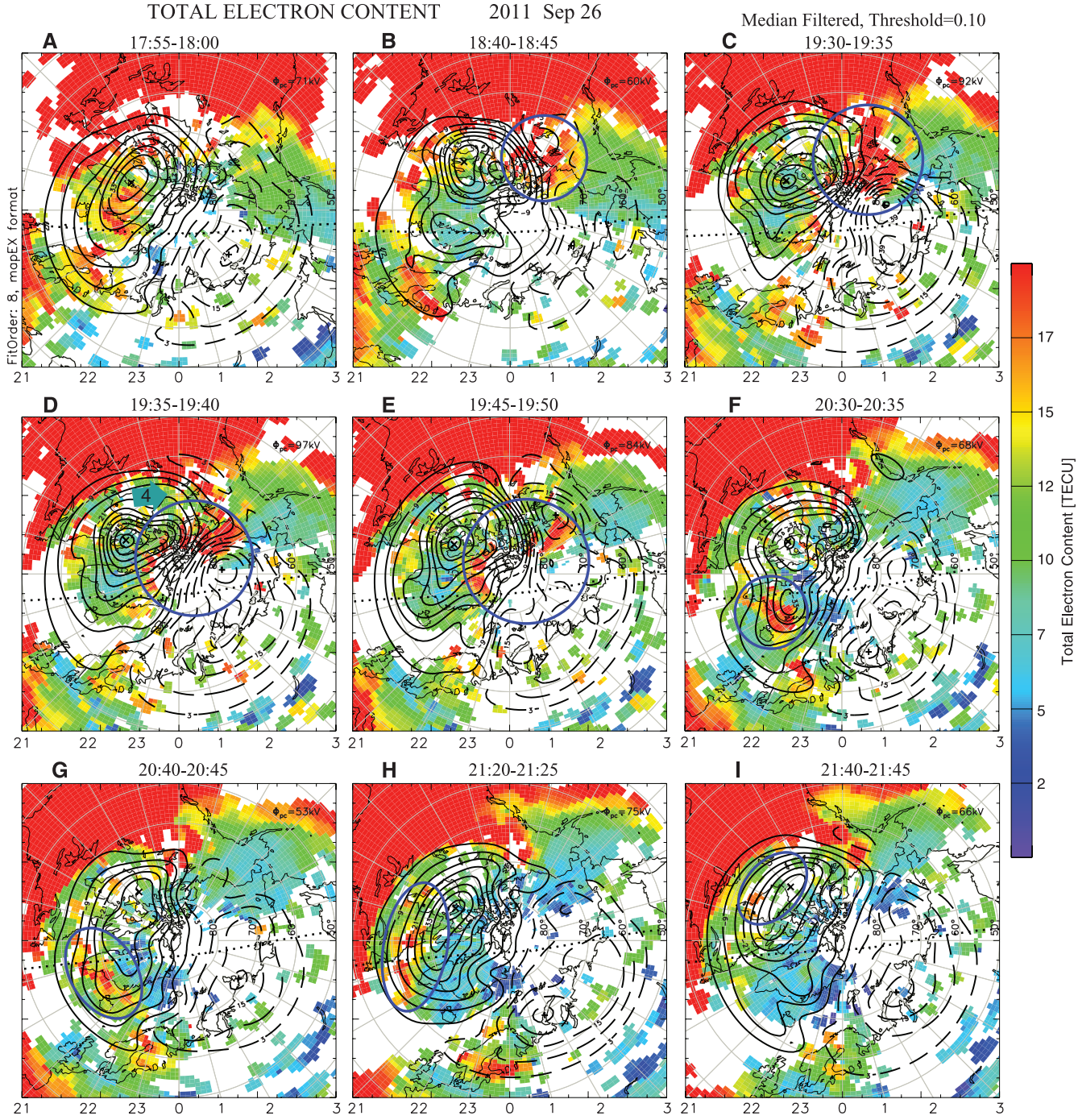

Fig. 2. (**A** to **I**) Extracts from a full series of 2D maps of median-filtered TEC (*24*) and ionospheric convection on a geomagnetic latitude/magnetic local time (MLT) grid with noon at the top (figs. S3 and S4 and movie S1). The dotted line across each panel is the day-night terminator at 100-km altitude. The blue circles and ellipses highlight the polar cap patch, the evolution of which is followed in this figure.

Figure 2 reveals the formation and evolution of a patch by mapping the TEC and flow streamlines. Figure 2A shows that the initial convection response was global, as discussed above, but as the IMF turned increasingly southward and the nightside reconnection voltage associated with the previous substorm decayed, the dominance of the dayside reconnection became apparent and the convection enhancement became more localized to the dayside (Fig. 2B) (*14*). After forming in the cusp region near noon (Fig. 2B), a large patch (ringed in blue) crossed through the throat, giving the local enhancement in TEC westward of the cusp. The strong positive IMF B_Y component implies westward flow in the throat; this has been invoked as a contributor to patch formation (*4*). The interval covered by Fig. 2, B and C, is the growth phase of the second substorm, during which the dayside polar cap boundary expanded equatorward (*26*), as predicted by the ECPC model. Such an expansion has been invoked as a cause of patch formation because the convection can move EUV-enhanced plasma toward the convection throat (*5*, *13*). However, the convection data show that the expansion occurred around 18:45 UT (fig. S2), which is after the patch formation began. Hence the polar cap expansion contributed to the continued growth of this patch, but its initial growth was due to rapid convection through the throat of high-TEC flux tubes in the near-noon auroral oval (which, from earlier TEC maps, can be attributed to a patch generated during the growth phase of the previous substorm that can be seen convecting sunward in the afternoon sector in Fig. 2A).

Interestingly, the patch seen forming in Fig. 2, B and C, did not directly move across the polar cap; rather, it was "stored" westward of the cusp region, where it grew in size: This is expected for a localized dayside convection enhancement, as seen in the SuperDARN convection patterns and as predicted by the ECPC model. Only when the convection enhancement expanded tailward (Fig. 2, D and E), did the patch migrate antisunward. The second substorm onset was between Fig. 2, B and C. (The patch appears to have bifurcated in Fig. 2E, but this is because there are no TEC data available poleward of 85°). The patch is completely separated from the high dayside TEC values by about 19:40 UT (Fig. 2E). It is useful to track back in time to define the evolution of the region of low TEC that "pinches off" the patch from the dayside: It can be seen to convect westward with the sunward return flow in the afternoon sector. Hence, these data answer the question of why this is a patch and not a TOI: It is pinched off by low TEC plasma in the post-noon auroral oval that is convected into the polar cap.

In Fig. 2, F to I, the patch is seen exiting the nightside auroral oval, breaking up into a number of plasma blobs, and moving sunward—as predicted in simulations—and returning sunward in the auroral oval of the dusk convection cell, which is consistent with the predictions from previous theories and trajectory analysis techniques (*16*, *17*). However, for the patch to exit the polar cap in this way requires ongoing nightside reconnection; without this, the open-closed boundary (OCB) would be "adiaroic" (Fig. 3), and the patch can only migrate slowly equatorward with the expanding polar cap boundary and, thus, would remain in the nightside polar cap (like the portion of the patch on the dusk convection cell in Fig. 3). Simulations show that the plasma recombination rates work on a time scale longer than the cycle time of plasma around polar cap cells, such that plasma concentrations convecting sunward in the auroral oval can be almost as large as in the newly formed patch in the dayside polar cap (*16*)—provided that tail reconnection allows the patch to exit the nightside polar cap. Nightside reconnection voltage dominates over dayside reconnection in substorm expansion phases, but is more restricted in rate and location (or even absent) during substorm growth phases (*27*). In addition, nightside reconnection may not be on the same cell (or even the streamlines within that cell) needed for reinjection into the polar cap in the cusp region. The ECPC model shows that, in a growth phase, the sunward-convecting regions are dominated by plasma that has been pushed sunward by the expanding polar cap but has not exited the polar cap through a reconnection site footpoint. Much of this plasma could have been in the dark for extended periods and so may be of low density. Thus, nightside reconnection, or more specifically the lack of it, has a key role to play in forming the gaps between patches, and this can explain why those gaps are larger if substorm activity is absent (*12*) and why patches can be segmented even before they enter the cusp region (*3*).

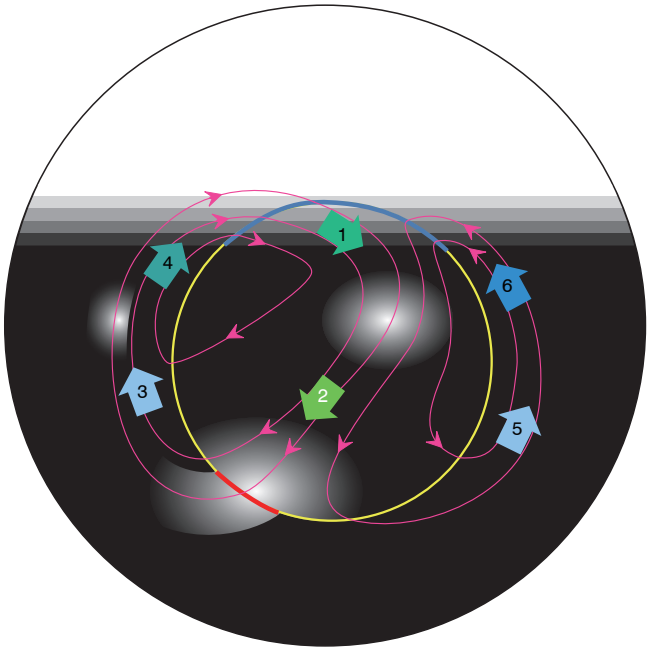

Fig. 3. Schematic of the northern polar ionosphere during a substorm growth phase with southward IMF and $B_Y > 0$. Convection streamlines are in mauve. The boundary between open and closed field lines lies close to the poleward edge of the auroral oval: the blue/red OCB segments show where magnetic reconnection at the magnetopause/magnetotail is generating/destroying open flux in the Dungey convection cycle (*9*). In this case, magnetopause reconnection is dominant and the polar cap is expanding (*18*). The yellow OCB segments are "adiaroic" (meaning "not flowing across") where flow streamlines cross the OCB because it is in motion and the plasma moves with it. The gray scale indicates plasma concentration, with white showing high values generated by solar EUV and black showing low values where plasma has decayed on the nightside. Convection leads to high-concentration plasma entering the polar cap from subauroral latitudes (arrow 1). The patches are transported antisunward across the polar cap (arrow 2) and evolve into "blobs". These have been seen leaving the polar cap on the nightside, but they can only do so at locations that map to ongoing magnetotail reconnection. Hence, in this case, although blobs are seen in part of the auroral sunward return flow region on the dusk side (arrows 3 and 4), they are absent completely from the corresponding region on the dawn side (arrows 5 and 6).

References and Notes

1. G. Crowley, *in Review of Radio Science 1992–1996*, W. Stone, Ed. (Oxford Univ. Press, Oxford, 1996), pp. 619–648.
2. H. C. Carlson, *Radio Sci.* **47**, RS0L21 (2012).
3. J. Moen *et al.*, *Ann. Geophys.* **24**, 2363 (2006).
4. Q. H. Zhang *et al.*, *J. Geophys. Res.* **116**, A05308 (2011).
5. M. Lockwood, H. C. Carlson Jr., *Geophys. Res. Lett.* **19**, 1731 (1992).
6. J. Moen, X. C. Qiu, H. C. Carlson, R. Fujii, I. W. McCrea, *Ann. Geophys.* **26**, 2427 (2008).
7. C. E. Valladares, D. Alcaydé, J. V. Rodriguez, J. M. Ruohoniemi, A. P. Van Eyken, *Ann. Geophys.* **17**, 1020 (1999).
8. A. S. Rodger, M. Pinnock, J. R. Dudeney, K. B. Baker, R. A. Greenwald, *J. Geophys. Res.* **99**, 6425 (1994).
9. The Dungey convection cycle is the flow of ionospheric plasma antisunward over the polar cap and the sunward return flow immediately outside the polar cap in the auroral ovals. It is caused by magnetopause reconnection, which generates "open" magnetic flux that is connected to the interplanetary magnetic field embedded in the solar wind flow and by reconnection in the cross-tail current sheet that recloses the flux, enabling it to migrate sunward back to the dayside. Steady state, in which these two reconnection voltages are equal, is rarely achieved, and the normal behavior is the substorm cycle in which magnetopause reconnection voltage dominates in the initial growth phase but the tail reconnection voltage dominates in the later expansion and recovery phases. The instantaneous ionospheric flow patterns for the

Dungey cycle during substorms are given by the ECPC model (*18*).
10. K. Oksavik, V. L. Barth, J. Moen, M. Lester, *J. Geophys. Res.* **115**, A12308 (2010).
11. K. Hosokawa *et al.*, *J. Geophys. Res.* **114**, A04318 (2009).
12. A. G. Wood, S. E. Pryse, J. Moen, *Ann. Geophys.* **27**, 3923 (2009).
13. M. Lockwood *et al.*, *Ann. Geophys.* **23**, 3513 (2005).
14. M. Lockwood *et al.*, *J. Geophys. Res.* **111**, A02306 (2006).
15. J. C. Foster *et al.*, *J. Geophys. Res.* **110**, A09S31 (2005).
16. J. J. Sojka *et al.*, *Geophys. Res. Lett.* **20**, 1783 (1993).
17. G. Crowley *et al.*, *J. Geophys. Res.* **105**, 5215 (2000).
18. S. W. H. Cowley, M. Lockwood, *Ann. Geophys.* **10**, 103 (1992).
19. G. S. Bust, G. Crowley, *J. Geophys. Res.* **112**, A05307 (2007).
20. TEC is the number of electrons present along a transionospheric path between two points, with units of electrons per square meter, where 10^{16} electrons/m^2 = 1 TEC unit (TECU) (*21*). TEC is important in determining the scintillation and group delay of radio waves passing through the ionosphere. It is determined by observing carrier phase delays of received radio signals transmitted from satellites above the ionosphere; here, we use GPS satellites. TEC is strongly affected by solar activity.
21. A. J. Coster, J. C. Foster, P. J. Erickson, *GPS World* **14**, 42 (2003).
22. C. Stolle *et al.*, *Ann. Geophys.* **24**, 107 (2006).
23. J. M. Ruohoniemi, K. B. Baker, *J. Geophys. Res.* **103**, (A9), 20797 (1998).
24. E. G. Thomas *et al.*, *J. Geophys. Res.*, (2013); 10.1002/jgra.50116
25. S. K. Morley, M. Lockwood, *Ann. Geophys.* **24**, 961 (2006).
26. M. Lockwood *et al.*, *Ann. Geophys.* **23**, 3495 (2005).
27. M. Lockwood, M. Hairston, I. D. Finch, A. P. Rouillard, *J. Geophys. Res.* **114**, A01210 (2009).

Acknowledgments: This work in China was supported by the National Basic Research Program (grant 2012CB825603), the National Natural Science Foundation (grants 41274149, 41104091, 41031064, and 40890164), and the Ocean Public Welfare Scientific Research Project, State Oceanic Administration (201005017). The Norwegian contribution was supported by the Research Council of Norway. SuperDARN is a collection of radars funded by national scientific funding agencies in Australia, Canada, China, France, Japan, South Africa, the United Kingdom, and the United States. The Virginia Tech authors acknowledge the support of NSF awards AGS-0946900 and AGS-0838219 and a graduate research fellowship from the Virginia Space Grant Consortium. The GPS TEC acquisition effort is led by A. J. Coster at MIT Haystack Observatory. The GPS TEC and SuperDARN data are available on the public database http://sd-software.ece.vt.edu/tiki/tiki-index.php?page=DaViT TEC. We also thank the NASA OMNIWeb for making available the solar wind/IMF data (http://omniweb.gsfc.nasa.gov/html/sc_merge_data1.html) and World Data Center C1, Kyoto, for the AE indices (http://wdc.kugi.kyoto-u.ac.jp/wdc/Sec3.html).

Supplementary Materials
www.sciencemag.org/cgi/content/full/339/6127/1597/DC1
Supplementary Text
Figs. S1 to S4
Movie S1
References

15 October 2012; accepted 31 January 2013
10.1126/science.1231487

Structure of the Integral Membrane Protein CAAX Protease Ste24p

Edward E. Pryor Jr.,[1,2]* Peter S. Horanyi,[1,2]* Kathleen M. Clark,[1,3]* Nadia Fedoriw,[1,3]* Sara M. Connelly,[1,3] Mary Koszelak-Rosenblum,[1,4] Guangyu Zhu,[1,4] Michael G. Malkowski,[1,4,5] Michael C. Wiener,[1,2]† Mark E. Dumont[1,3,6]†

Posttranslational lipidation provides critical modulation of the functions of some proteins. Isoprenoids (i.e., farnesyl or geranylgeranyl groups) are attached to cysteine residues in proteins containing C-terminal CAAX sequence motifs (where A is an aliphatic residue and X is any residue). Isoprenylation is followed by cleavage of the AAX amino acid residues and, in some cases, by additional proteolytic cuts. We determined the crystal structure of the CAAX protease Ste24p, a zinc metalloprotease catalyzing two proteolytic steps in the maturation of yeast mating pheromone a-factor. The Ste24p core structure is a ring of seven transmembrane helices enclosing a voluminous cavity containing the active site and substrate-binding groove. The cavity is accessible to the external milieu by means of gaps between splayed transmembrane helices. We hypothesize that cleavage proceeds by means of a processive mechanism of substrate insertion, translocation, and ejection.

Isoprenoid groups are conjugated to proteins by means of cysteine residues of CAAX acceptor sequences in which the cysteine attachment site is followed by two aliphatic amino acid residues and one unspecified residue at the protein C terminus. Isoprenylation is generally accompanied by two subsequent processing steps, proteolytic cleavage of the AAX residues and carboxymethylation of the newly exposed carbonyl group of the modified cysteine residue (fig. S1). Some isoprenylated proteins also undergo additional proteolytic processing, including an additional cleavage by the same protease that initially removes the AAX residues. At least two classes of enzymes are responsible for the cleavage of isoprenylated proteins and peptides. One of these is the Ras-converting enzyme (Rce) family of type II prenyl proteases, responsible for proteolytic processing of signal-transducing proteins including Ras (*1*, *2*) and the G_γ subunits of heterotrimeric GTP-binding protein (G protein) complexes (*3*). The other is the Ste24p family of type I prenyl proteases, first identified in yeast on the basis of its role in maturation of the mating pheromone **a**-factor (*4*–*6*). Extensive characterization of the role of Ste24p in **a**-factor processing has been conducted in the yeast system (*7*). Ste24p is localized to the endoplasmic reticulum membrane. Its proteolytic activity requires zinc, consistent with the fact that Ste24p contains the zinc metalloprotease signature motif HEXXH (*8*, *9*).

A human ortholog of Ste24p, zinc metalloprotease STE24 (ZMPSTE24), can complement the full function of yeast Ste24p (*6*). The only known substrate for ZMPSTE24 is prelamin A, the precursor to the nuclear intermediate filament protein lamin A. Lamins provide mechanical stability to the nuclear envelope, function as scaffolds for localization of other proteins and for cytoskeletal attachment, regulate chromatin, and are implicated in transcription and DNA repair and replication (*10*). Mutations in either ZMPSTE24 or the processing site of prelamin A are associated with a spectrum of premature-aging diseases referred to as progeria (*11*). The severity of different forms of progeria is reported to be correlated with extent of loss of ZMPSTE24 activity (*12*). Also, ZMPSTE24 (and *Saccharomyces cerevisiae* Ste24p) are inhibited by antiviral drugs designed to target the HIV aspartyl protease, and this off-target interaction may give rise to some of the severe side effects of these drugs (*13*, *14*).

Ste24p from *Saccharomyces cerevisiae* (ScSte24p) has been overexpressed previously in *S. cerevisiae* cells and purified (*9*, *15*). To identify forms of the protein with enhanced stability and suitability for crystallization, we cloned and purified orthologs from nine yeast species closely related to *S. cerevisiae*. *S. mikatae* Ste24p (SmSte24p) is 96% identical to ScSte24p and is 37% identical to *H. sapiens* ZMPSTE24 (fig. S2). Purified SmSte24p is enzymatically active (fig. S3), and we obtained crystals of this protein that diffracted anisotropically to 3.1 Å resolution (and isotropically to 3.9 Å resolution). After obtaining a native data set and proceeding to make selenomethionine-containing SmSte24p (*16*), we discovered that the Structural Genomics Consortium (SGC) had solved the structure of human ZMPSTE24. Because of SGC's open access policy, the coordinates were deposited in the Protein Data Bank (PDB) before publication [PDB: 4AW6 (*17*)]. Thus, we solved the structure of SmSte24p by a combination of molecular replacement (MR) and single-wavelength anomalous diffraction (SAD) of the bound catalytic zinc atoms.

[1]Membrane Protein Structural Biology Consortium, USA. [2]Department of Molecular Physiology and Biological Physics, Box 800886, University of Virginia, Charlottesville, VA 22908–0886, USA. [3]Department of Pediatrics, Box 703, University of Rochester School of Medicine and Dentistry, Rochester, NY 14642, USA. [4]Hauptman-Woodward Institute, 700 Ellicott Street, Buffalo, NY 14203, USA. [5]Department of Structural Biology, State University of New York at Buffalo, 700 Ellicott Street, Buffalo, NY 14203, USA. [6]Department of Biochemistry and Biophysics, Box 712, University of Rochester School of Medicine and Dentistry, Rochester, NY 14642, USA.

*These authors contributed equally to this work.
†Corresponding author. E-mail: mwiener@virginia.edu (M.C.W.); mark_dumont@urmc.rochester.edu (M.E.D.)